ACS APPLIED MATERIALS & INTERFACES

Research Article

www.acsami.org

Synthesis of Bacteria Promoted Reduced Graphene Oxide-Nickel Sulfide Networks for Advanced Supercapacitors

Haiming Zhang, Xinzhi Yu, Di Guo, Baihua Qu, Ming Zhang, Qiuhong Li,* and Taihong Wang*

Key Laboratory for Micro-Nano Optoelectronic Devices of Ministry of Education, and State Key Laboratory for Chemo/Biosensing and Chemometrics, Hunan University, Changsha 410082, China

Supporting Information

ABSTRACT: Supercapacitors with potential high power are useful and have attracted much attention recently. Graphene-based composites have been demonstrated to be promising electrode materials for supercapacitors with enhanced properties. To improve the performance of graphene-based composites further and realize their synthesis with large scale, we report a green approach to synthesize bacteria-reduced graphene oxide-nickel sulfide (BGNS) networks. By using *Bacillus subtilis* as spacers, we deposited reduced graphene oxide/Ni_3S_2 nanoparticle composites with submillimeter pores directly onto substrate by a binder-free electrostatic spray approach to form BGNS networks. Their electrochemical capacitor performance was evaluated. Compared with stacked reduced graphene oxide-nickel sulfide (GNS) prepared without the aid of bacteria, BGNS with unique nm−μm structure exhibited a higher specific capacitance of about 1424 F g^{-1} at a current density of 0.75 A g^{-1}. About 67.5% of the capacitance was retained as the current density increased from 0.75 to 15 A g^{-1}. At a current density of 75 A g^{-1}, a specific capacitance of 406 F g^{-1} could still remain. The results indicate that the reduced graphene oxide-nickel sulfide network promoted by bacteria is a promising electrode material for supercapacitors.

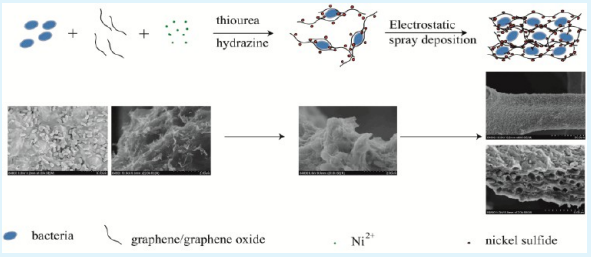

KEYWORDS: *nickel sulfide, reduced graphene oxide, bacteria, supercapacitors, nm−μm structure*

1. INTRODUCTION

Supercapacitors have drawn much attention because of their potential applications in energy storage devices to complement or replace batteries in high-power applications.[1−5] However, the defects of traditional electrode materials (carbon material, and polymers) have seriously hindered their practical applications in high-performance supercapacitors. Although transitional metal oxides can provide higher specific capacitance than conventional carbon materials and better electrochemical stability than polymer materials, the poor intrinsic properties of these metal oxide materials still seriously limits their performance.[6] Compared with conventional electrode materials, metal sulfides (e.g., NiS_x, CuS_x, and CoS_x) are receiving more and more attention as electrode materials for supercapacitors due to their interesting intrinsic properties.[7−11] The family of nickel sulfides with different phases such as NiS and Ni_3S_2 have been studied as electrode materials.[7,9,10] For example, Lou and co-workers have reported hierarchical NiS hollow spheres, which manifested interesting supercapacitive properties of 927 F g^{-1} at 4.08 A g^{-1} and 583 F g^{-1} at 10.2 A g^{-1}.[9] However, their cycling performance are less satisfactory due to pulverization of electrode materials during cycling, which leads to the breakdown of electrical connection of electrode materials from current collectors. Two feasible methods have been developed to improve the electrochemical properties of supercapacitors, including preparing graphene-based composites and synthesizing materials directly supported on current collectors.[2,5,6,11−15]

Graphene-based composites usually were stacked and harmful for the transfer of ions in them. Recently, researchers have recognized the tremendous merits of porous graphene due to the increase of active material per unit area.[16−21] Some reports have been focused on incorporating spacers such as CNTs,[19,20] carbon spheres,[17,18] polystyrene nanoparticles,[21] and silica spheres[22] into the graphene layers. The existence of spacers can improve the electrolyte-electrode accessibility, ensure the high electrochemical utilization of graphene sheets and maintain the open channels. However, traditional methods always require several steps to synthesize and modify the spacers first, leading to the whole process with high cost, environmental unfriendliness, and time consumption. Thus it is highly appealing to establish a general method with inexpensive, efficient, and environmentally friendly spacers for the synthesis of porous graphene-based composites. Lu and co-workers developed an approach for producing bioinspired hierarchically structured graphene by combining the assembly of graphene oxide (GO) on the surface of bacteria with a freeze-casting technique.[3] However, Lu's work and many other graphene-based composites were focused on synthesizing composite

Received: May 6, 2013
Accepted: June 10, 2013
Published: June 10, 2013

powders, followed by mixing them with conductive additives and binders to fabricate the electrode.[3,11] Part of the active material surface was blocked from the contact with electrolyte, which would increase the resistivity and dead weight to the electrode. Preparing of graphene-based electrode material directly supported on current collector can be more favorable than traditional binder-contained methods.

Moreover, among all the approaches developed to date, the difficulty of preparation materials in large scale still exists.[12,23] For an attempt to address both green and large scale synthesis of composites for supercapacitors with high properties, we investigated an approach involving electrostatic spray deposition (ESD) of *Bacillus subtilis* promoted BGNS networks. Gram-positive bacteria, *Bacillus subtilis*, acted as spacers to prepare reduced graphene oxide networks with submillimeter pores, Ni_3S_2 nanoparticles (~10 nm) were uniformly anchored onto both sides of the graphene sheets to form a unique nm−μm structure. The BGNS was deposited directly onto substrates by a binder-free ESD approach. Moreover, we evaluated their electrochemical capacitor performance. Compared with GNS, BGNS with unique nm−μm structure exhibited better performance. The improvement was mainly attributed to the structure promoted by bacteria, which greatly improved the diffusion kinetics within the electrode.

2. EXPERIMENTAL SECTION

Materials. Graphite powders were purchased from Alfa Aesar China (Tianjin) Co. Ltd. Nickel acetate tetrahydrate ($Ni(CH_3COO)_2{\cdot}4H_2O$) and thiourea were purchased from Sinopharm Chemical Resgent Co. Ltd. (Shanghai, China). All other chemicals were of analytical grade and used as received without any purification process. The water was Millipore Milli-Q grade with a resistivity larger than 18 MΩ cm^{-1}.

Preparation of GO. GO was prepared from graphite powders based on a modified Hummers' method,[24] as reported previously.[25,26] Then, exfoliation was achieved by sonicating the GO dispersion for 2 h (400 W). Finally, a homogeneous GO aqueous dispersion (1 mg mL^{-1}) was obtained.

Preparation of BGNS, GNS, and NF. Gram-positive bacteria, *Bacillus subtilis* were cultured in a liquid medium of the LuriaBertani broth at 310 K. The bacterial cells were centrifuged at 8000 rpm for 5 min and resuspended in distilled water to adjust the optical density (OD 600 nm) to 1.5, similar to our previous report.[27] Forty microliters of bacteria was mixed with an aqueous solution of 2 mmol of nickel acetate, and then 40 mL of GO was added in. After exposure to ultrasound for 30 min, 2 mmol of thiourea, 2 mL of hydrazine monohydrate, and 60 mL of ethylene glycol were added and the mixture was heated to 431 K followed by stirring for 4 h. The resulting product was separated by centrifugation, washed three times, and then dispersed in ethanol with the assistance of ultrasonication at room temperature. The as-prepared solution was transferred to a syringe. The nickel foam (1 cm × 1 cm, carefully cleaned with acetone, ethanol, and deionized water in an ultrasound bath) was used as a substrate and the distance between the needle and the substrate was 3−5 cm. While applying a direct current (DC) voltage of 10−20 kV between the substrate and the needle, the flow rate to feed the precursor solution was controlled at 1−3 mL h^{-1} by a syringe pump. During the deposition, the nickel foam substrate was heated to 353 K. After deposition, the black nickel foam was carefully rinsed several times with the assistance of ultrasonication, and finally dried in vacuum at 333 K. The composite was named as BGNS and ~1.3 mg of BGNS was obtained per 1 cm × 1 cm area (carefully weighted before and after deposition, the weight increase was defined as the mass of active material). The same mass loading of GNS (without the addition of bacteria) was also obtained by adjusting the deposition time. Considering a possible oxidation of nickel foam during deposition and to evaluate the capacitance contributed from the substrate, pure ethanol was deposited onto the bare nickel foam at 353 K, and it was named NF.

Characterization. The morphologies of the composite were characterized by scanning electron microscopy (SEM) [Hitachi S-4800], transmission electron microscope (TEM), and high-resolution transmission electron microscope (HRTEM) [JEOL2010]. Fourier transform infrared (FTIR) spectra of the samples were obtained on a WQF-410 Fourier transform infrared spectrophotometer (Beijing Secondary Optical Instruments, China). The crystal structure of the samples was characterized by X-ray diffraction (XRD) [Rigaku Dmax-2500]. Raman spectra were taken on a LabRAM HR 800 Raman spectrometer. Thermogravimetric analysis (TGA, Setaram018124) was performed in air at a heating rate of 10 K min^{-1} ranging from 323 K to 1073K.

Electrochemical Tests. The nickel foam-supported composites were directly used as the working electrode with a platinum plate counter electrode and Hg/HgO as the reference electrode by using a CHI 660D electrochemical workstation. The electrolyte was a 2 M KOH aqueous solution.

The specific capacitance (C) is calculated from the chronopotentiometry curves based on the following equation:

$$C = It/V$$

where I, t, and V are discharging current density, discharging time and discharging potential range, respectively.

Electrochemical impedance spectroscopies (EIS) tests were carried out with a frequency loop from 1 × 10^5 Hz to 0.1 Hz with perturbation amplitude of 5 mV under the open-circuit potential.

3. RESULTS AND DISCUSSIONS

The BGNS films were prepared in two steps: fabrication of Ni_3S_2-reduced graphene oxide-bacteria composites and electrostatic spray of the composites onto the surface of nickel foam (Scheme 1). First, *Bacillus subtilis* cells (Scheme 1a) with the diameter of 0.4−0.6 μm and length of 1−2 μm were mixed with nickel acetate and graphene oxide. The surface charge of GO and bacteria are both negative due to the groups on their surfaces.[3,28] With the help of positive Ni^{2+}, bacteria would be

Scheme 1. Schematic Illustration for the Synthesis of BGNS

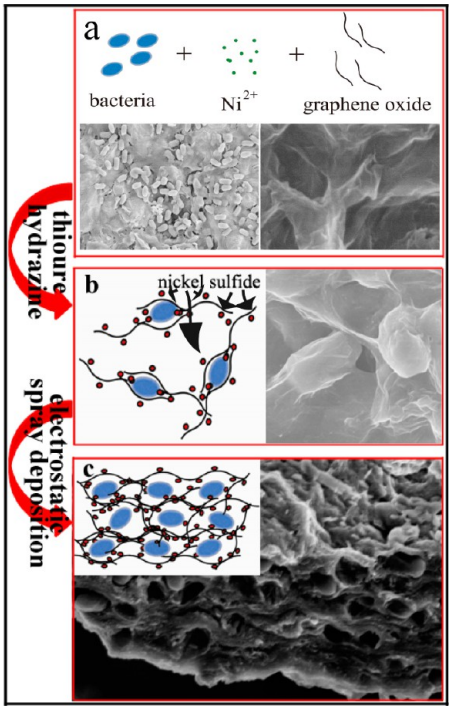

dx.doi.org/10.1021/am401680m | ACS Appl. Mater. Interfaces 2013, 5, 7335−7340

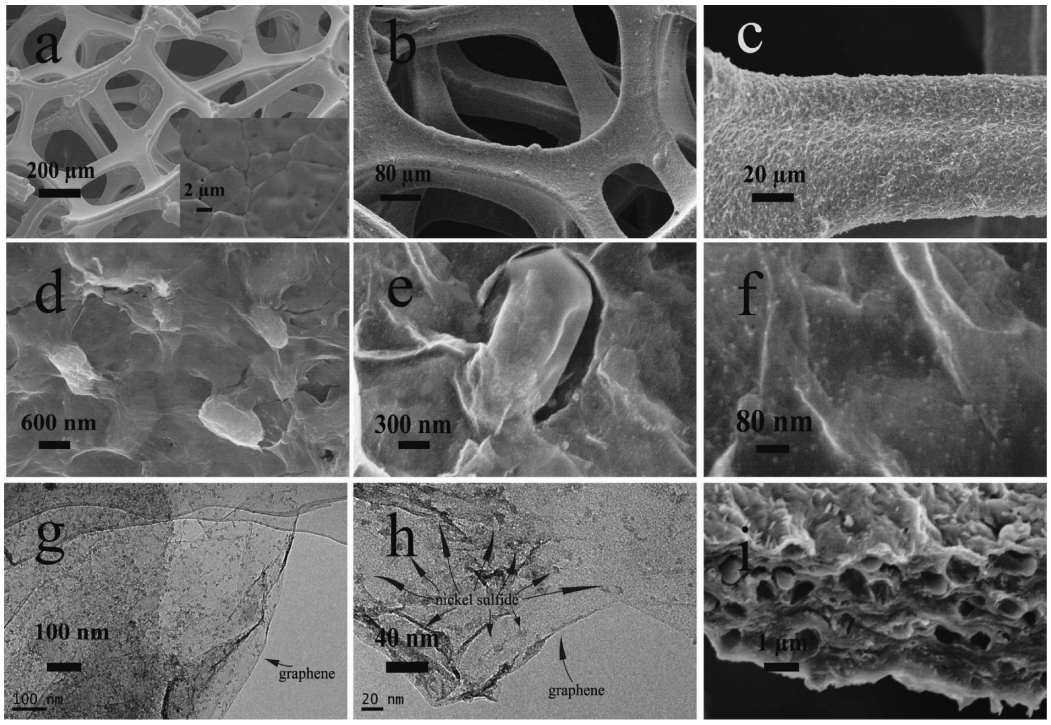

Figure 1. Top view of SEM images at different magnifications, (a) NF, inset, a close view of NF and (b–f) BGNS, (g, h) TEM images of BGNS at different magnifications, (i) typical cross-sectional SEM image of BGNS.

electrostatic interacted between graphene oxide sheets to form bacteria–Ni^{2+}–graphene oxide composites.[3] At the same time, plenty of positive Ni^{2+} are anchored on both surfaces of the graphene oxide. Then, thiourea was added and the whole reaction procedure could be expressed as follows[29]

$$GO + N_2H_4 \rightarrow \text{reduced graphene oxide}$$

$$Ni^{2+} + N_2H_4 \rightarrow [Ni(N_2H_4)_3]^{2+}$$

$$[Ni(N_2H_4)_3]^{2+} + N_2H_4 \rightarrow Ni + 4NH_3 + 2N_2 + H_2 + 2H^+$$

$$NH_2CSNH_2 + 2H_2O \rightarrow 2NH_3 + H_2S + CO_2$$

$$3Ni + 2H_2S \rightarrow Ni_3S_2 + 2H_2$$

The SEM image of the composites (Scheme 1b) indicates that the bacteria cell were wrapped by graphene and plenty of nickel sulfide particles were anchored on the reduced graphene oxide sheets. The composites were dispersed in ethanol by ultrasonication at room temperature and transferred to a syringe for deposition.[19,30] Herein, bacteria-reduced graphene oxide-nickel sulfide composites were electrostatic spray deposited onto the surface of substrate, such as nickel foam. The SEM image of nickel foam supported composites in Scheme 1c displayed a porous structure. The structure severed as a robust reservoir for ions, and greatly enhanced the diffusion kinetics within the electrode. The digital photographs of BGNS supported on nickel foam and bacteria-reduced graphene oxide-nickel sulfide composites solution (see Figure S1 in the Supporting Information) indicate that the whole process can be scalable. Moreover, the composites can be deposited onto different substrates such as carbon fabric cloth and stainless steel disk (see Figure S2 in the Supporting Information), further indicating that the ESD technology is a feasible choice for large-scale synthesis of graphene-based composites supported on different substrates.

The morphology of bare nickel foam and BGNS was examined by SEM and TEM as shown in Figure 1. The submillimeter pores and nickel foam skeletons can be clearly seen in Figure 1a and the nickel grains of the skeletons are observable at a higher magnification (inset in Figure 1a). Figure 1b–f display the SEM images of BGNS supported on nickel foam. The nickel foam surfaces are uniformly covered with porous BGNS network,s and the reduced graphene oxide wrinkles and bacteria are clearly identified. A close view of the film indicates that the bacteria cells are covered by reduced graphene oxide sheets (Figure 1d–e) and the nickel sulfide nanoparticles are uniformly loaded on the surface of reduced graphene oxide (Figure 1e, f). The typical size of nickel sulfide nanoparticles is about 10 nm, which can be further confirmed by the TEM images g and h in Figure 1. Cross-sectional SEM images of BGNS are displayed in Figure 1i, and large numbers of submicrometer pores are observed in the BGNS film. The diameter of the pores matches well with that of bacteria spacers and some bacteria can still be observed in the pores. The unique composite nm–μm structure would be helpful to its potential application. A completely different morphology is observed from GNS (see Figure S3 in the Supporting Information), which further demonstrates that the bacteria plays a key role for the formation of a porous structure. The bacteria promoted nm–μm structure can maintain an open surface between reduced graphene oxide sheets, thus improving the accessibility of ions from electrolyte to inner active regions of the electrode during charging and discharging.

Figure 2 shows XRD pattern of the BGNS film. The three sharp peaks are indexed to the nickel substrate. The other minor peaks could be attributed to Ni_3S_2 (JCPDS 44–1418). No diffraction peak assigned to graphene is found in the

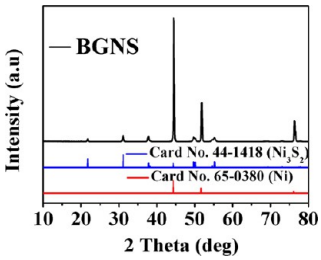

Figure 2. XRD patterns of BGNS.

patterns of composites, because the content of graphene in BGNS is low.

Both GO and BGNS are investigated by Raman spectroscopy, as displayed in Figure 3a. The peak at about 1592 cm^{-1}

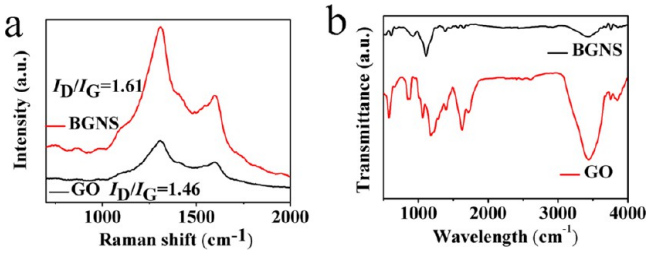

Figure 3. (a) Raman and (b) FT-IR spectra for GO and BGNS.

(G band), corresponding to an E_{2g} mode of graphite, is related to the vibration of the sp^2-bonded carbon atoms in a two-dimensional hexagonal lattice, and the peak at about 1327 cm^{-1} (D band) is related to the defects and disorder in the hexagonal graphitic layers.[25] The intensity ratio of the D band to the G band (I_D/I_G) reflects the graphitization degree of carbonaceous materials and the defect density,[25,26] and was calculated to be 1.46 for GO and 1.61 for BGNS. Compared with GO, the increased I_D/I_G can be attributed to the presence of unrepaired defects after the removal of partial oxygen moieties and the separated graphene layers promoted by the intercalation of bacteria and nickel sulfide nanoparticles. The FT-IR spectra of GO confirmed the presence of oxygen-containing groups, such as C−OH (at 3400 cm^{-1}), C−O−C (at 1230 cm^{-1}), and C═O in carboxylic acid moieties (at 1730 cm^{-1}).[31] Other characteristic peaks at 1400 and 1055 cm^{-1} could be ascribed to the O−H deformation peak and the C−O stretching, respectively. The peak at 1620 cm^{-1} was assigned to the skeletal vibrations of the graphitic domains.[32] As for BGNS, the characteristic absorption peaks of oxygen-containing groups (C−OH, C−O−C, and C═O) decreased dramatically, indicating that GO had been reduced to reduced graphene oxide.[26]

To explore the advantages of BGNS as an electrode material for supercapacitors, we analyzed its electrochemical properties by cyclic voltammograms (CV) and galvanostatic charge/discharge techniques using a three-electrode system. It should be noted that the mass loading of BGNS and GNS were similar by adjusting the deposition time. Figure 4a revealed that the CV curve of BGNS-based electrode materials presented a pair of strong redox peaks, which indicated that the capacitance characteristics were mainly governed by Faradaic redox reactions, quite distinct from that of bacteria promoted hierarchical carbon materials that presented a CV curve close to an rectangular shape.[3] Suggesting that nickel sulfide plays the

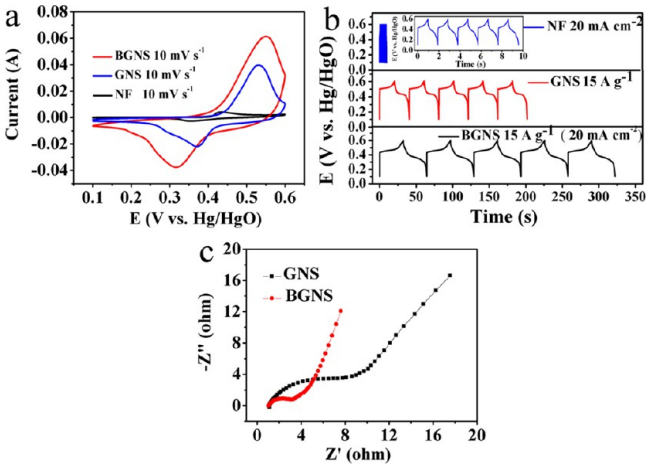

Figure 4. (a) CV and (b) galvanostatic charge/discharge curves of NF, GNS, and BGNS. (c) Nyquist plots of GNS and BGNS.

key role to the total capacitance rather than the reduced graphene oxide or bacteria. Under the same testing conditions, the CV curve of GNS showed smaller encircled area, suggesting that with the help of bacteria, the BGNS had a higher capacitance. The capacitive behavior of BGNS and GNS was also confirmed by galvanostatic charge/discharge curves, as shown in Figure 4b. Compared with GNS, BGNS displayed a longer charge/discharge time, implying a larger capacitance. This was consistent with the CV curve results. The EIS analysis is generally used to predict the behavior of electrochemical capacitor, and to determine the parameters affecting the performance of an electrode.[33] In the low frequency area, the slope of the curve shows the Warburg impedance which represents the electrolyte diffusion in the porous electrode and proton diffusion in host materials. BGNS showed lower diffusion resistance (Figure 4c), which could be attributed to its porous structure.[34] In the high-frequency area, the intersection of the curve at real part indicates the bulk resistance of the electrochemical system (electrolyte resistance, intrinsic resistance of substrate, and contact resistance at the active material/current collector interface), and the semicircle (corresponds to double layer capacitance and charge-transfer resistance) displays the charge-transfer process at the working electrode−electrolyte interface.[35] The charge-transfer resistance is related to the electroactive surface area of electrode materials for the Faradaic reaction to occur. The larger the electroactive surface area, the lower the charge transfer resistance.[33] As shown in Figure 4c, BGNS displayed lower charge-transfer resistance than GNS. It is believed that the combination of low diffusion and electron-transfer resistances are responsible for the improved electrochemical performance of BGNS.[35] Considering a possible capacitance contribution from NF besides the active material composites, the electrochemical properties of NF were analyzed by CV and galvanostatic charge/discharge techniques. The CV curve of NF displayed a much smaller encircled area than that of GNS and BGNS, suggesting that the capacitance attributed to NF was very small. Similar to the CV curve results, the discharge time of NF (less than 1 s) was much smaller than that of BGNS (about 32 s) at the same current density (20 mA cm^{-2}). Both CV and galvanostatic charge/discharge results indicated that the capacitance of the electrode was mainly attributed to the active material.

Scheme 2 illustrated the schematic of GNS and BGNS during charging and discharging. Although reduced graphene

Scheme 2. Schematic Illustration of GNS and BGNS during Charging and Discharging; (a) Reduced Graphene Oxide Sheets Aggregate and Stack into a Layered Structure; It Is Difficult for Electrolyte to Reach the Inner Part of the GNS Film; (b) Bacteria Act As Spacers to Increase the Interlayer Spacing between Reduced Graphene Oxide Sheets, Thus Making the Inner Part of Nickel Sulfide Particles Electrochemically Active

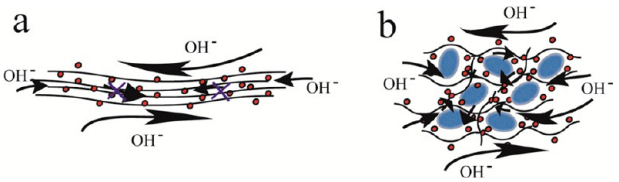

oxide-nickel sulfide could be well-dispersed in aqueous solution, upon drying, the isolated sheets easily aggregated and formed an irreversibly precipitated agglomerate. This agglomeration could decrease the active surface area and preclude the access of electrolyte ions into the inner parts of GNS, which further deteriorated its performance. For BGNS, the bacteria acted as spacers to increase the interlayer spacing between reduced graphene oxide sheets, with nickel sulfide nanoparticles uniformity anchored onto the separated reduced graphene oxide sheets, a unique μm−nm structure was success prepared. The nm−μm structure greatly improved the diffusion kinetics within the electrode, making the inner part of nickel sulfide particles electrochemically active. Thus, the porous BGNS exhibited better performance than GNS.

Figure 5a showed CV analysis at various scan rates in the potential range of 0.1−0.6 V (vs Hg/HgO). These CV profiles clearly reveal pronounced pseudocapacitive characteristics different from the nearly rectangular CV shapes for conventional electric double-layer capacitors.[33] Rate capability is an important feature for supercapacitors, and we investigated the rate-dependent galvanostatic discharge curves for BGNS over a

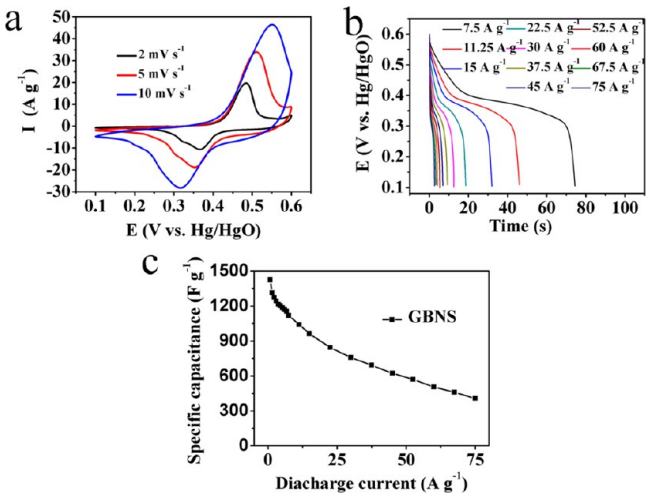

Figure 5. Electrochemical characterization of BGNS. (a) CV curves at different scan rates, (b) galvanostatic discharge curves at different current densities, and (c) specific capacitance calculated from the discharge curves.

wide range of current densities from 7.5 to 75 A g^{-1} as shown in Figure 5b. The plateau region observed in the discharge process corresponded to the cathode process. With the increase of current density, the capacitance was gradually reduced (Figure 5c). And the specific capacitances calculated from the discharge curves are 1424, 1315, 1272, 1242, 1215, 1202, 1185, 1169, 1154, 1119, 1040, 962, 844, 758, 692, 623, 568, 505, 460, and 406 F g^{-1} at current densities of 0.75, 1.5, 2.25, 3, 3.75, 4.5, 5.25, 6, 6.75, 7.5, 11.25, 15, 22.5, 30, 37.5, 45, 52.5, 60, 67.5, and 75 A g^{-1}, respectively. This suggested that about 67.5% of the capacitance was still retained as the current density increased from 0.75 to 15 A g^{-1}. At a higher current density of 75 A g^{-1}, a specific capacitance of 406 F g^{-1} can still remain. Compared with previous reports, such as Ni_3S_2 nanosheets grown on carbon nanotube,[10] nickel sulfide hollow spheres[9] and NiS nanoparticles,[7] our BGNS exhibited a better performance.

The cycle life of supercapacitors is a crucial parameter for their practical application. To investigate the electrochemical stability of BGNS and GNS, galvanostatic charge/discharge measurements were performed at a current density of 15 A g^{-1}. The columbic efficiency of BGNS was nearly 100% for each cycle of charge and discharge (see Figure S5 in the Supporting Information). After continuously cycling for 3000 cycles at 15 A g^{-1}, 89.6% of the initial capacitance was still delivered (Figure 6). For comparison, GNS was conducted at the same current

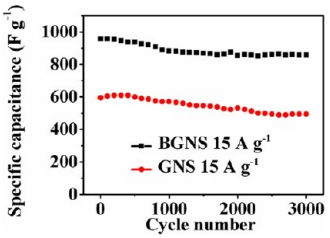

Figure 6. Cycling performance of BGNS and GNS at the same current density.

density. About 83.0% of the initial capacitance was delivered after 3000 cycles. This value is lower than that of BGNS but better than that of previous report.[9]

The excellent performance could be attributed to the novel structure of the composite electrode with the help of bacteria. First, Ni_3S_2 nanoparticles about 10 nm were directly anchored on reduced graphene oxide sheets, resulting in an intimate contact between the nanoparticles and reduced graphene oxide sheets, which afforded a facile electron transport in the composite. Second, the structure promoted by bacteria severed as a robust reservoir for ions, which greatly improved the diffusion kinetics within the electrode. Last, the binder-free nature of the electrode resulted in a direct contact of the conductive BGNS film with nickel foam substrate, which built up an express path for fast electron transport. Thus most of the Ni_3S_2 nanoparticles in the macroscopic ensemble were electrochemically active through the network. The results indicate that the bacteria promoted porous Ni_3S_2-reduced graphene oxide structure is a promising electrode material for supercapacitors.

4. CONCLUSION

In conclusion, the *Bacillus subtilis* promoted porous nickel sulfide-reduced graphene oxide composites directly supported

dx.doi.org/10.1021/am401680m | ACS Appl. Mater. Interfaces 2013, 5, 7335−7340

on nickel foam was realized by a green and binder-free ESD approach. Ni_3S_2 nanoparticles (~10 nm) are uniformly anchored onto reduced graphene oxide sheets with submillimeter pores. The composites with unique nm-μm structure exhibited excellent electrochemical capacitor performance, about 1424 F g^{-1} at a current density of 0.75 A g^{-1}, and about 67.5% of the capacitance was retained as the current rate increased from 0.75 to 15 A g^{-1}. At a higher current density of 75 A g^{-1}, a specific capacitance of 406 F g^{-1} could still remain. After continuously cycling for 3000 cycles at 15 A g^{-1}, 89.6% of the initial capacitance was delivered. The results indicate that preparing porous graphene composites on current collectors by ESD with the aid of bacteria is a promising approach to synthesize high property electrode materials for supercapacitors. The strategy developed in this work would open up a general approach of producing porous graphene-based composite film for high-performance energy-storage devices.

■ ASSOCIATED CONTENT

Supporting Information

Digital photographs of BGNS supported on nickel foam and bacteria-reduced graphene oxide-nickel sulfide composites solution; Digital photographs and SEM images of BGNS supported on stainless steel disk and carbon fabric cloth; SEM images of GNS. TGA curve of BGNS; The galvanostatic charge−discharge curves of BGNS; Cross-sectional SEM image of graphene wrapped bacteria (BG), CV curves of BG and BGNS after 3000 cycles. Galvanostatic discharge curves from 0.75 to 7.5 A g^{-1}. XRD pattern of the BGNS after 3000 cycles. This material is available free of charge via the Internet at http://pubs.acs.org.

■ AUTHOR INFORMATION

Corresponding Author

*E-mail:liqiuhong2004@hotmail.com (Q.L.); thwang@iphy.ac.cn (T.W.). Tel.: +86 0731 888664020 (Q.L.); +86 0731 88823407 (T.W.). Fax: +86 0731 88822137 (Q.L.); +86 0731 88823407 (T.W.).

Notes

The authors declare no competing financial interest.

■ ACKNOWLEDGMENTS

This work was supported by the National Natural Science Foundation of China (Grants 21003041 and 21103046), the Specialized Research Fund for the Doctoral Program of Higher Education of China (Grants 20120161110016), and the Hunan Provincial Natural Science Foundation of China (Grants 10JJ1011 and 11JJ7004).

■ REFERENCES

(1) Malvankar, N. S.; Mester, T.; Tuominen, M. T.; Lovley, D. R. *ChemPhysChem* **2012**, *13*, 463−468.
(2) Jiang, J.; Li, Y. Y.; Liu, J. P.; Huang, X. T.; Yuan, C. Z.; Lou, X. W. *Adv. Mater.* **2012**, *24*, 5166−5180.
(3) Sun, H. M.; Cao, L. Y.; Lu, L. H. *Energy Environ. Sci.* **2012**, *5*, 6206−6213.
(4) Guo, C. X.; Li, C. M. *Energy Environ. Sci.* **2011**, *4*, 4504−4507.
(5) Liu, J. P.; Jiang, J.; Cheng, C. W.; Li, H. X.; Zhang, J. X.; Gong, H.; Fan, H. J. *Adv. Mater.* **2011**, *23*, 2076−2081.
(6) Zhang, G. Q.; Lou, X. W. *Adv. Mater.* **2012**, *25*, 976−979.
(7) Hou, L. R.; Yuan, C. Z.; Li, D. K.; Yang, L.; Shen, L. F.; Zhang, F.; Zhang, X. G. *Electrochim. Acta* **2011**, *56*, 7454−7459.
(8) Zhu, T.; Xia, B. Y.; Zhou, L.; Lou, X. W. *J. Mater. Chem.* **2012**, *22*, 7851−7855.
(9) Zhu, T.; Wang, Z. Y.; Ding, S. J.; Chen, J. S.; Lou, X. W. *RSC Adv.* **2011**, *1*, 397−400.
(10) Zhu, T.; Wu, H. B.; Wang, Y. B.; Xu, R.; Lou, X. W. *Adv. Energy Mater.* **2012**, *2*, 1497−1502.
(11) Qu, B. H.; Chen, Y. J.; Zhang, M.; Hu, L. L.; Lei, D. N.; Lu, B. A.; Li, Q. H.; Wang, Y. G.; Chen, L. B.; Wang, T. H. *Nanoscale* **2012**, *4*, 7810−7816.
(12) Candelaria, S. L.; Shao, Y. Y.; Zhou, W.; Li, X. L.; Xiao, J.; Zhang, J. G.; Wang, Y.; Liu, J.; Li, J. H.; Cao, G. Z. *Nano Energy* **2012**, *1*, 195−220.
(13) Wu, Z. S.; Ren, W. C.; Wang, D. W.; Li, F.; Liu, B. L.; Cheng, H. M *ACS Nano* **2010**, *4*, 5835−5842.
(14) Takahashi, K.; Wang, Y.; Cao, G. Z. *J. Phys. Chem. B* **2005**, *109*, 48−51.
(15) Wu, Z. S.; Zhou, G. M.; Yin, L. C.; Ren, W. C.; Li, F.; Cheng, H. M. *Nano Energy* **2012**, *1*, 107−131.
(16) Zhang, J. T.; Jiang, J. W.; Li, H. L.; Zhao, X. S. *Energy Environ. Sci.* **2011**, *4*, 4009−4015.
(17) Lei, Z. B.; Christov, N.; Zhao, X. S. *Energy Environ. Sci.* **2011**, *4*, 1866−1873.
(18) Guo, C. X.; Li, C. M. *Energy Environ. Sci.* **2011**, *4*, 4504−4507.
(19) Beidaghi, M.; Wang, C. L. *Adv. Funct. Mater.* **2012**, *22*, 4500−4509.
(20) Tung, V. C.; Chen, L. M.; Allen, M. J. *Nano Lett.* **2009**, *9*, 1949−1955.
(21) Choi, B. G.; Yang, M. H.; Hong, W. H.; Choi, J. W.; Huh, Y. S. *ACS Nano* **2012**, *6*, 4020−4028.
(22) Huang, X. D.; Qian, K.; Yang, J.; Zhang, J.; Li, L.; Yu, C Z.; Zhao, D. Y. *Adv. Mater.* **2012**, *24*, 4419−4423.
(23) Candelaria, S. L.; Chen, R.; Jeong, Y. H.; Cao, G. Z. *Energy Environ. Sci.* **2012**, *5*, 5619−5637.
(24) Hummers, W. S.; Offeman, R. E. *J. Am. Chem. Soc.* **1958**, *80*, 1339−1339.
(25) Zhang, M.; Lei, D. N.; Yin, X. M.; Chen, L. B.; Li, Q. H.; Wang, Y. G.; Wang, T. H. *J. Mater. Chem.* **2010**, *20*, 5538−5543.
(26) Zhang, M.; Qu, B. H.; Lei, D. N.; Chen, Y. J.; Yu, X. Z.; Chen, L. B.; Li, Q. H.; Wang, Y. G.; Wang, T. H. *J. Mater. Chem.* **2012**, *22*, 3868−3874.
(27) Zhang, H. M.; Xu, C.; Sheng, P. K.; Chen, Y. J.; Yu, L.; Li, Q. H. *Sens. Actuators, B* **2013**, *181*, 99−103.
(28) Akin, D.; Sturgis, J.; Ragheb, K.; Sherman, D.; Burkholder, K.; Robinson, J. P.; Bhunia, A. K.; Mohammed, S.; Bashir, R. *Nat. Nanotechnol.* **2007**, *2*, 441−449.
(29) Zhang, Y. H.; Guo, L.; He, L.; Liu, K.; Chen, C. P.; Zhang, Q.; Wu, Z. Y. *Nanotechnology* **2007**, *18*, 485609.
(30) Beidaghi, M.; Wang, Z. F.; Gu, L.; Wang, C. L. *J. Solid State Electrochem.* **2012**, *16*, 3341−3348.
(31) Liang, Y. Y.; Wu, D. Q.; Feng, X. L.; Müllen,, K. *Adv. Mater.* **2009**, *21*, 1679−1683.
(32) Si, Y. C.; Samulski, E. T. *Nano Lett.* **2008**, *8*, 1679−1682.
(33) Wu, M. S.; Wang, M. J.; Jow, J. J. *J. Power Sources* **2010**, *195*, 3950−3955.
(34) Wang, K. P.; Teng, H. S. *J. Electrochem. Soc.* **2007**, *154*, A993−A998.
(35) Guan, C.; Liu, J. P.; Cheng, C. W.; Li, H. X.; Li, X. L.; Zhou, W. W.; Zhang, H.; Fan, H. J. *Energy Environ. Sci.* **2011**, *4*, 4496−4499.